Check for updates

View Article Online
View Journal

Nanoscale
Advances

Accepted Manuscript

This article can be cited before page numbers have been issued, to do this please use: M. H. Carvalho, D. Zau, A. P. Reyes, R. Cong, S. D. House, H. Pizzi, A. M. Caffer, D. L. Passos, R. Santos, G. Freitas, K. R. Pirota, R. R. Urbano and P. G. Pagliuso, *Nanoscale Adv.*, 2026, DOI: 10.1039/D6NA00173D.

Nanoscale
Advances

Volume 1
Number 1
January 2018
Pages 1-200

rsc.li/nanoscale-advances

ISSN 2516-0230

ROYAL SOCIETY
OF CHEMISTRY

NCNST

This is an Accepted Manuscript, which has been through the Royal Society of Chemistry peer review process and has been accepted for publication.

Accepted Manuscripts are published online shortly after acceptance, before technical editing, formatting and proof reading. Using this free service, authors can make their results available to the community, in citable form, before we publish the edited article. We will replace this Accepted Manuscript with the edited and formatted Advance Article as soon as it is available.

You can find more information about Accepted Manuscripts in the Information for Authors.

Please note that technical editing may introduce minor changes to the text and/or graphics, which may alter content. The journal's standard Terms & Conditions and the Ethical guidelines still apply. In no event shall the Royal Society of Chemistry be held responsible for any errors or omissions in this Accepted Manuscript or any consequences arising from the use of any information it contains.

ROYAL SOCIETY
OF CHEMISTRY

rsc.li/nanoscale-advances

ROYAL SOCIETY OF CHEMISTRY
View Article Online
DOI: 10.1039/D6NA00173D

ARTICLE TYPE

Cite this: DOI: 00.0000/xxxxxxxxxx

Dramatic Suppression of Antiferromagnetic Ordering in $CeIn_3$ Nanowires[†]

Maria H. Carvalho,*[ab] Davi Zau[a], Arneil P. Reyes[c], Rong Cong[c], Stephen D. House[d], Henrique P. Pizzi[a], Ana M. Caffer[a], Derick S. Passos[a], Rodolfo C. Santos[a], Gabriel S. Freitas[b], Kleber R. Pirota[a], Ricardo R. Urbano[a], Pascoal J. G. Pagliuso [ab]

Received Date
Accepted Date

DOI: 00.0000/xxxxxxxxxx

In this work, we have employed the Metallic-Flux Nanonucleation method to synthesize $CeIn_3$ nanowires (diameter $\approx$ 175 nm) and single crystals for comparison. The physical properties of the nanowires were systematically investigated using Energy Dispersive Spectroscopy (EDS), Selected Area Electron Diffraction (SAED), magnetic susceptibility, heat capacity, and Nuclear Magnetic Resonance (NMR). Semi-quantitative EDS analysis revealed a Ce:In ratio of 1:3.1(1), and the SAED results confirmed that the nanowires are polycrystalline with a cubic unit cell. Magnetic susceptibility, specific heat, and NMR data indicated a suppression of the antiferromagnetic transition to $T_N \approx 2.4$ K compared to the bulk value ($\approx$ 10 K). Furthermore, NMR analysis at temperatures below 2.8 K showed a reduced quadrupole frequency, $\nu_Q \approx 1.77(2)$ MHz, and provided evidence of polycrystalline nanowires formed within the nanoporous alumina template, in agreement with SAED results. We attribute these findings to an increase in magnetic frustration, induced by disorder and the confinement of $CeIn_3$ within the nanometric pores of the alumina template.

1 Introduction

Materials science is one of the main pillars of scientific and technological development. To make progress in this area, two strategies are generally important: i) novel materials design and ii) engineering known materials into new forms, shapes, and devices. In the latter, producing known materials in thin films, nanowires and/or nanoparticle forms is a particularly interesting route which has been the focus of intense efforts by the materials community for decades[1–4].

In particular, in the quantum size limit, when one of the dimensions of the system becomes comparable to a fundamental length scale, the disruption of translational symmetry can alter the material's ground state. Furthermore, in reduced spatial dimensions, many-body correlation effects become more pronounced, as Coulomb interactions between electrons play an increasingly dominant role in the behavior of the material[5–8].

On the other hand, even well above the quantum size limit which is usually a few lattice parameters, engineering materials in 2D and 1D form using templates and/or substrates can introduce distortions, dislocations, stress/strains, and other defects that can also significantly alter the ground state of the materials in a similar way to applying external hydrostatic/uniaxial pressure and/or chemical substitutions in 3D materials. This is particularly relevant when the energy scales of the material are very sensitive to the subtle changes in the crystal or electronic structure[9].

In Ce-based intermetallic heavy fermions (HF) materials, f electrons hybridize with conduction electrons, and the Ruderman–Kittel–Kasuya–Yosida (RKKY) interaction, which favors long-range magnetic order, typically competes with the Kondo effect. As a result of this competition, a tuning of a magnetically ordered state toward a quantum phase transition at $T = 0$ may occur. The balance of both interactions can be tuned by external parameters such as doping[10], magnetic field[11,12], applied pressure[13,14], and, of interest here, reduced dimensionality[15]. Unconventional superconductivity (USC) and Non-Fermi liquid behavior often occur in the vicinity of such quantum critical points[16].

The comparative study on the series $Ce_mM_n\ In_{3m+2n}$ ($M =$ Co, Rh, Ir; $n = 0, 1$; $m = 1, 2$) previously allowed the investigation of the role of dimensionality in these compounds even in single crystal form. For $m = 1$ and $n = 0$, three-dimensional (3D) cubic compound $CeIn_3$ that presents an antiferromagnetic (AFM) ordering, $T_N \approx 10$ K at ambient pressure, and undergoes a transition to a superconducting state ($T_C = 0.2$ K) at critical pressure $P \approx 25$ kbar[13,14]. For $m = 1$ and $n = 1$, one finds the more two-dimensional (2D) tetragonal compounds $CeMIn_5$, so-called 115, which presents alternating layers of Ce-In_3 and M-In_2 along the c axis[17]. Depending on the transition metal element M, the 115 compounds can be unconventional superconductors, e.g. $M =$ Co, $T_C = 2.3$ K or $M =$ Ir, ($T_C \approx 0.4$ K),[18,19] or antiferromagnetic (AFM) $M =$ Rh, with $T_N = 3.8$ K, at atmospheric pressure,

---

[a] Instituto de Física Gleb Wataghin, UNICAMP, Campinas-SP, 13083-859, Brazil. E-mail: helenacc@unicamp.br
[b] Los Alamos National Laboratory, Los Alamos, New Mexico 87545, USA
[c] National High Magnetic Field Laboratory, Tallahassee, Florida 32310, USA
[d] Center for Integrated Nanotechnologies (CINT), Sandia National Laboratories, New Mexico 87185, USA

[†] Supplementary Information available: Electronic supplementary information (ESI) available. See DOI: 00.0000/00000000.

View Article Online
DOI: 10.1039/D6NA00173D

and becoming superconducting only under applied pressure[17]. From these studies, it has been argued that unconventional superconductivity generated by magnetic fluctuations tends to be favored in the 2D 1-1-5 families, while AFM is favored for 3D bulk materials[17]. Rare earth metal (RE)In$_3$ compounds have already been studied in the literature extensively[12,20–24]. However, these compounds have been underexplored when it comes to tuning their form/dimensionality in a controllable way, from 3D to 2D and 1D. One of the pioneering studies in this direction reported the growth by molecular beam epitaxy of 2D CeIn$_3$/LaIn$_3$ heterostructures. The suppression of the magnetic order of CeIn$_3$ was observed with the reduction of the thickness of the CeIn$_3$ layers and the effective electron mass was further enhanced. In addition, the 2D confined heterostructures showed low-temperature deviations of the electronic properties from Fermi-liquid behavior, which were associated with the dimensional tuning of quantum criticality[15]. Furthermore, Rosa et al. performed a study on the effect of dimensionality on the physical properties of the intermetallic compound GdIn$_3$ using the Metallic-Flux Nanonucleation (MFNN) method to obtain this compound in nanowire form. Magnetic susceptibility and specific heat measurements showed a drastic suppression of the AFM order temperature ($T_N^{3D} = 45$ K) of the single crystal bulk to a $T_N^{LD} = 3.8$ K for the nanowire system (diameter d $\approx$ 200 nm and length l $\approx$ 30 μm). Since Gd^{3+} is a pure spin $S = 7/2$ ion ($L = 0$), such reduction was associated with a suppression of the RKKY magnetic interaction[25]. The cubic intermetallic HF compound CeIn$_3$ is an excellent compound to understand, and ultimately control, quantum phenomena in f-based low-dimensional systems, as it presents a variety of interesting physical properties, such as RKKY magnetic interaction, Kondo effect, crystalline electric field (CEF), non-Fermi-liquid behavior and the interaction between antiferromagnetism and unconventional superconductivity. However, the growth of intermetallic nanowires containing a rare-earth element has been challenging[25–34].

After intense efforts,[26] we report a successful route to synthesize CeIn$_3$ nanowires with diameter of 175(25) nm by the MFNN method. The crystal structure and stoichiometry of the nanowires were investigated by Energy Dispersive X-ray Spectroscopy (EDS) and Selected Area Electron Diffraction (SAED). In addition, the temperature dependence of the magnetic susceptibility and specific heat of an Al$_2$O$_3$ template with the CeIn$_3$ nanowires was determined to obtain the nanowires macroscopic properties. Importantly, to gain microscopic insights into the properties of the CeIn$_3$ nanowires, we have employed the Nuclear Magnetic Resonance (NMR) technique to investigate the microscopic nature of the relevant interactions in the nanowire system.

Our results reveal a drastic suppression of the antiferromagnetic transition from the bulk ($T_N^{3D} = 10$ K) to the CeIn$_3$ low-dimensional systems ($T_N^{LD} = 2.3$ K) as similarly observed in their GdIn$_3$ counterparts[25]. In particular, the NMR results reported here clearly indicate a disordered AFM state below T_N arising from an arrangement of polycrystalline CeIn$_3$ nanowires.

We discuss this suppression of T_N due to an increase of frustration of the magnetic order for an array of polycrystalline disordered nanowires, taking into account how the relevant interactions such as RKKY exchange interactions, crystalline electric field, and Kondo effect evolve from the bulk to nanowires of CeIn$_3$ in the presence of disorder.

These observations indicate that by engineering CeIn$_3$ in a more 1D form, significantly altered its properties, motivating further strategies to explore the role of changes in form/dimensionality in the properties of strongly correlated materials.

2 Experimental methods

2.1 Synthesis method

The CeIn$_3$ nanowires were grown by the Metallic Flux Nanonucleation (MFNN) method[3,35]. This method is a combination of the conventional metallic flux-growth technique[36] with the addition of a nanometric template for nanowire ingrowth, which provides simultaneous growth of nanowires and bulk crystals in the same batch, facilitating the comparative study of dimensionality effects on the properties of the compounds. Particularly, in this work, we used an Al$_2$O$_3$ membrane as a template with a pore size of 156(25) nm fabricated by the hard anodization process described in detail in Ref.[37]. The broad pore size distribution of the alumina template arises from post-anodization processing, including chemical etching during barrier layer removal and pore widening, combined with a heat treatment at 900°C for 2 h to induce membrane crystallization. The template was added together with the metals in a ratio of 1 Ce:10 In inside a quartz tube, with the addition of quartz wool at the extremities of the tube to remove excess In. The sealed evacuated tube was placed in a furnace and heated up to 1100°C at a rate of 50°C/h. After 8h at 1100°C, the batch was cooled to 800°C at a rate of 1°C/h, and finally to 650°C at 10°C/h. The excess In flux was then spun in a centrifuge, and the membrane with nanowires and the CeIn$_3$ crystals were mechanically removed from the quartz tube. The CeIn$_3$ nanowires exhibit sufficient short-term stability under ambient conditions to allow handling during sample preparation and subsequent characterization procedures. However, to prevent progressive surface oxidation, long-term storage was carried out under an inert atmosphere (Ar atmosphere glovebox), consistent with the behavior observed for bulk CeIn$_3$ single crystals.

2.2 Techniques and Analysis

CeIn$_3$ bulk and nanowires were analyzed with a commercial Quanta FEG 250 Field Emission Scanning Electron Microscope (FE-SEM) and submitted to elemental analysis using a commercial Energy Dispersive X-Ray Spectroscopy (EDS) microprobe model X-Max50. The Selected Area Electron Diffraction (SAED) patterns in the transmission electron microscope (TEM) were performed in a FEI Titan ETEM equipped with an image Cs corrector and a Gatan K3-IS direct detection counting camera, operated at 300 kV. For SAED analysis, a lamella was prepared from the CeIn$_3$ nanowires using a dual-beam focused ion beam/scanning electron microscope (FIB) from Thermo Fisher Helios 600 Nanolab Ga$^+$ FIB/SEM - equipped with an OmniProbe micro-manipulator. Magnetization data were collected using a superconducting quantum interference device (SQUID) magnetometer MPMS-7T. Spe-

View Article Online
DOI: 10.1039/D6NA00173D

cific heat data (12 K to 0.3 K) were taken in a commercial Quantum Design PPMS using a ^{3}He system. NMR measurements were performed on a ^{3}He cryostat equipped with a variable 17 T superconducting magnet at the National High Magnetic Field Laboratory (NHMFL) in Tallahassee-FL. A radio frequency coil was manufactured with a formvar insulating copper wire to perform low-T NMR measurements at $40-50$ MHz. The same alumina template with the CeIn$_3$ nanowires used in the macroscopic measurements was mounted on an NMR probe equipped with a goniometer for fine alignment with the external field. The field-swept ^{115}In NMR spectra ($I = 9/2$; $\gamma/2\pi = 9.3295$ MHz/T) were obtained by stepwise summing the Fourier transform of the spin-echo signal. The NMR data were collected using a MagRes2000 homodyne spectrometer. To analyze the magnetic susceptibility and specific heat in CeIn$_3$ single crystals and nanowires, we adopted a mean-field (MF) model[23]. The model incorporates the CEF Hamiltonian of a Ce^{3+} ion and isotropic first-neighbors interactions between local moments, that mimic the Ruderman-Kittel-Kasuya-Yosida (RKKY) interaction. This MF model has been successfully used in previous investigations of Ce-based heavy-fermion compounds[23,38,39]. The Hamiltonian is written as:

$$\mathscr{H} = K\sum_{i,j}\mathbf{J}_i\cdot\mathbf{J}_j - \mu\cdot\mathbf{B} + B_2^0O_2^0 + B_4^0O_4^0 + B_4^4O_4^4 \tag{1}$$

where the term $K > 0$ denotes an antiferromagnetic nearest-neighbor local spin $\mathbf{J_i}$, the second term accounts for the Zeeman effect, and the last terms correspond to the B_n^m CEF parameters and O_n^m equivalent Stevens operators[40]. A standard mean-field approximation ($\mathbf{J}_i\cdot\mathbf{J}_j \approx z\mathbf{J}\cdot\langle\mathbf{J}\rangle$), where z is the number of nearest neighbors, is employed, allowing the interaction term of the Hamiltonian to be simplified to $zK\mathbf{J}\cdot\langle\mathbf{J}\rangle$. We considered two isotropic interactions between nearest and next-nearest neighbors.

3 Results and Discussion

3.1 Electron microscopy

Fig. 1 shows the high-resolution Scanning Electron Microscope (FE-SEM) image and Energy Dispersive X-ray Spectrometry (EDS) mapping of a small area of the Al$_2$O$_3$ template containing nanowires. Fig 1(a) shows an electron back-scatter diffraction (EBSD) image that clearly reveals the atomic number contrast of the regions filled with CeIn$_3$ nanowires and the Al$_2$O$_3$ template. We observed the presence of CeIn$_3$ nanowires with an average diameter of 175(25) nm. The EDS characterization (Fig. 1c-f) confirms that the synthesized sample is composed only of Ce, In, Al and O. The semi-quantitative analysis of the atomic composition performed experimentally for Ce and In yields a ratio of 1:3.1(1) compared to the nominal ratio of 1:3, which supports the formation of CeIn$_3$. For SAED analysis, a lamella was prepared with a cross-sectional cut inside the CeIn$_3$ nanowires (Fig. 1a) using Ga$^+$ FIB, and placed on a copper (Cu) TEM grid, as illustrated in Fig. 2(a). To reduce beam-induced damage, the final thinning steps involved low kV (2 kV) thinning with a current of 27 pA. Fig. 2(b) shows a TEM image of the CeIn$_3$ lamella, displaying the cross section of the nanowires, which shows a length distribution $\approx 1-2\mu$m.

We performed SAED on the region of Fig. 2(c) with at least 4 nanowires, to investigate the crystal structure and obtain the lattice parameters. The SAED pattern, Fig. 2(d), exhibits a polycrystalline character, and the indexing reveals the presence of the cubic structure of CeIn$_3$ with space group Pm-3m. We obtained the lattice parameter a = b = c = 4.75(5) Å, which is in fair agreement with the value of 4.69 Å, reported for CeIn$_3$ bulk[41], considering the experimental accuracy. The apparent difference of approximately 1% is likely due to Pt re-deposition, ion implantation or another impurity incorporation mechanism commonly generated during the preparation of the FIB lamella[42].

3.2 Physical Characterization

We now turn our attention to the evolution of the physical properties of the CeIn$_3$ compound going, from the bulk to nanowire form. For both single crystals and nanowire arrays embedded in the alumina template, the magnetic susceptibility $\chi(T)$ was measured as a function of temperature under an applied magnetic field of $H = 0.1$T, as shown in Fig. 3(a) and (b), respectively. To isolate the contribution of the nanowires, a reference measurement of an empty Al$_2$O$_3$ template[26] was performed and subtracted from the total signal of the nanowires/template system. The resulting susceptibility was then normalized by the molar mass of CeIn$_3$.

For both bulk and LD systems, the inverse molar magnetic susceptibility as a function of temperature $\chi(T)^{-1}$ above 150 K can be fitted to a Curie-Weiss law plus a T-independent term, (χ_0), accounting for the contributions from Pauli paramagnetism and core diamagnetism, $\chi(T) = \chi_0 + C/(T-\theta_{CW})$ (see inset of Fig. 3(a,b)). Table 1 shows the fitting parameters. The effective moment (p_{eff}) for the Ce^{3+} ions, extracted from the Curie-Weiss constant (C), is in very good agreement with $p_{eff}^{theory} = 2.54\ \mu_B$ from the Hund's rule moment for free J = 5/2 cerium ions[43]. This, along with the lattice constants obtained from SAED analyses, confirms the formation of CeIn$_3$ nanowires in the Al$_2$O$_3$ template. The negative sign of θ_{CW} indicates an antiferromagnetic interaction, consistent with an antiferromagnetic ground state of CeIn$_3$. Interestingly, the reduction of the high-T θ_{CW} for the nanowires may indicate a suppression of the long-range AFM exchange interaction in the CeIn$_3$ nanowires. Additionally, $|\theta_{CW}| > T_N$ for both systems, indicating the presence of magnetic frustration, as previously observed for GdIn$_3$ nanowires[25]. The ratio θ_{CW}/T_N is higher for the LD system, implying a more pronounced frustration in the nanowire than in the bulk system. In addition, magnetization as a function of magnetic field, M(H), measured at 2 K (data not shown) shows linear behavior for both bulk CeIn$_3$ and the nanowires, as expected for an antiferromagnetic state, with no significant size dependence. However, the most significant finding from our data is the substantial reduction of T_N by a factor of 4 in the nanowire system compared to the bulk one. Similarly, previous studies corresponding to larger diameters (≈ 350 nm) reported a less pronounced suppression of the magnetic ordering temperature to $T_N \approx 3$ K[26]. This comparison indicates a size-dependent trend, in which reducing the

View Article Online
DOI: 10.1039/D6NA00173D

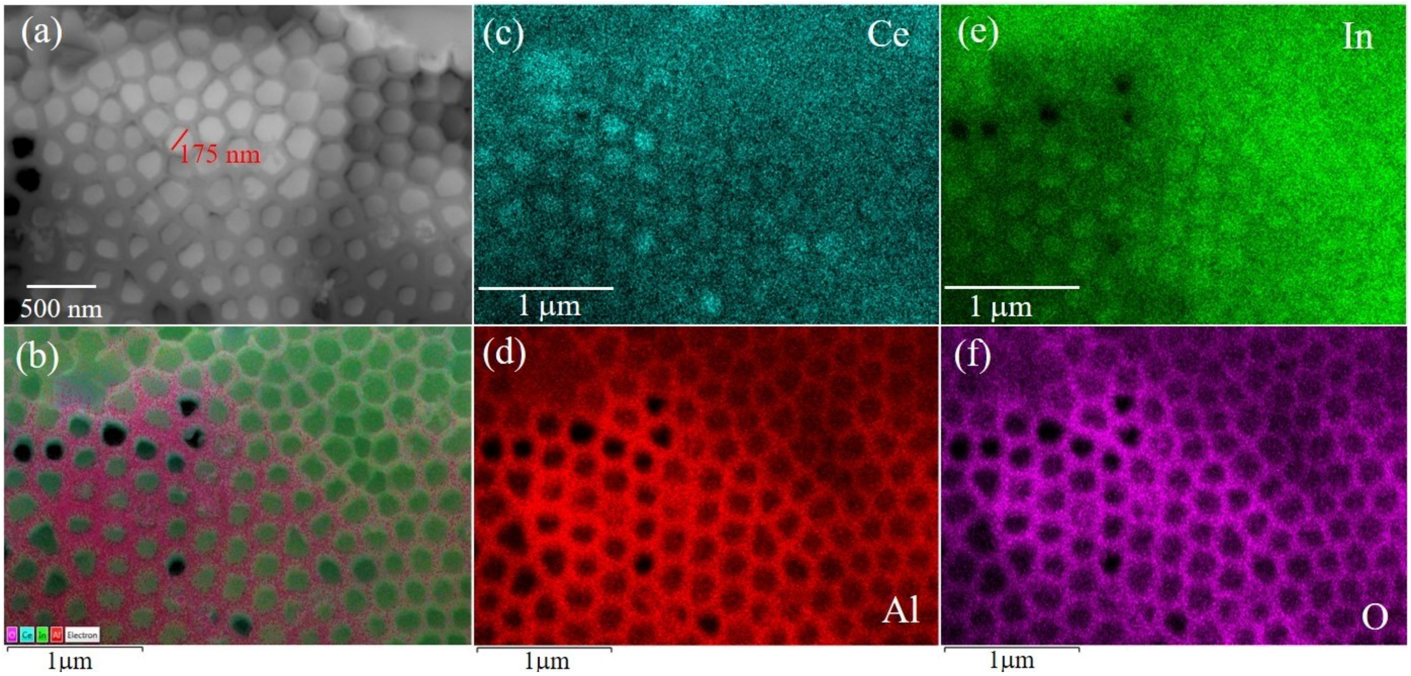

Fig. 1 (a) Electron back-scatter diffraction (EBSD) image showing the atomic number contrast of the $CeIn_3$ nanowires and the Al_2O_3 template; (b) Image reconstructed from the EDS mapping of Figures (c-f).

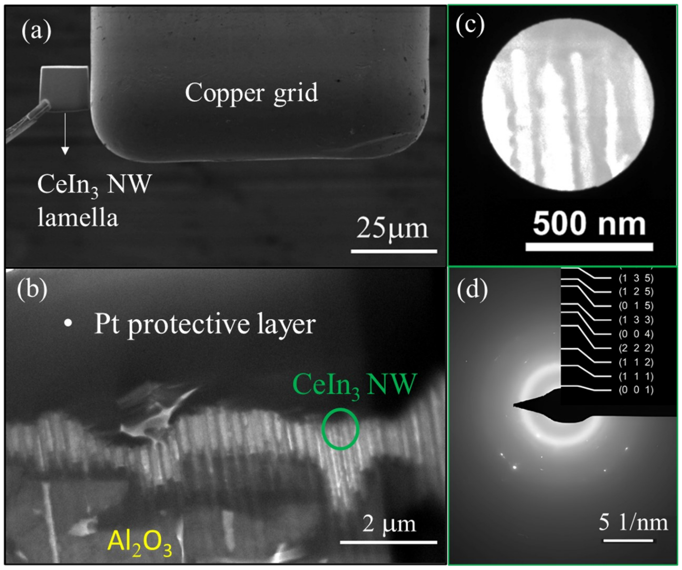

Fig. 2 (a) SEM image of a $CeIn_3$ lamella. (b) TEM image of the cross-section of the nanowires, showing the contrast of the Pt layer, the $CeIn_3$ nanowires, and the Al_2O_3 template. (c,d) SAED pattern of the nanowires. Inset highlights the region where the SAED was performed.

dimensionality increases the deviation from bulk magnetic behavior.

The solid lines in Fig. 3(a,b) correspond to the best fit to the bulk and NW $CeIn_3$ data and additional simulations of these data using our CEF Hamiltonian mean-field model, which will be further discussed later on to understand the behavior observed in nanowires.

The suppression of the magnetic order at T_N is confirmed by specific heat measurements. Fig. 4(a) shows the total specific heat, C divided by temperature, as a function of temperature, $C/T \times T$, for $CeIn_3$ nanowires and bulk. For the nanowire, a reference measurement of the empty Al_2O_3 template was performed and subtracted from the total signal to isolate the contribution of the nanowires. The sharp peaks in C/T corresponding to the onset of the AFM order can be seen at 10.1 K for the bulk and at 2.3 K for the nanowires, consistent with the maximum identified in the magnetic susceptibility data (see Fig. 3(a,b)). These results clearly show a pronounced suppression of the AFM ordering temperature in the nanowire system.

Table 1 Curie-Weiss fitting parameters for both bulk and nanowire $CeIn_3$ systems with $\chi(T) = \chi_0 + C/(T-\theta_{CW})$.

$CeIn_3$	$\theta_{CW}(K)$	χ_0 (emu/mol.Oe)	p_{eff} (μ_B)	$\frac{\theta_{CW}}{T_N}$
Bulk	-43(1)	$2.0(1)\times10^{-4}$	2.54(1)	4
Nanowire	-24(4)	$3.5(6)\times10^{-4}$	2.59(5)	10

Estimated entropy S as a function of T for the bulk and $CeIn_3$ nanowires are shown in Fig. 3(d). The solid lines were calculated from the CEF parameters extracted from the best fit using our CEF Hamiltonian mean-field model on magnetic susceptibility data. The corresponding total entropy $[S = \int (C/T)\,dT]$ is obtained by integrating the total contribution to the specific heat up to 12 K. Only for single crystals did we obtain magnetic entropy S_{mag} after subtraction of the non-magnetic contribution of $LaIn_3$ from the C_p data. The S_{mag} (12 K) is $\approx 83\%$ of $R\ln 2$ for $CeIn_3$ suggesting a slightly compensated doublet CEF ground-state for the Ce^{3+} ion, in agreement with previous reports[23,44,45]. On the other hand, for $CeIn_3$ NW, the entropy recovered at T_N is only roughly 0.5 $R\ln 2$, which indicates a higher Kondo compensation

View Article Online
DOI: 10.1039/D6NA00173D

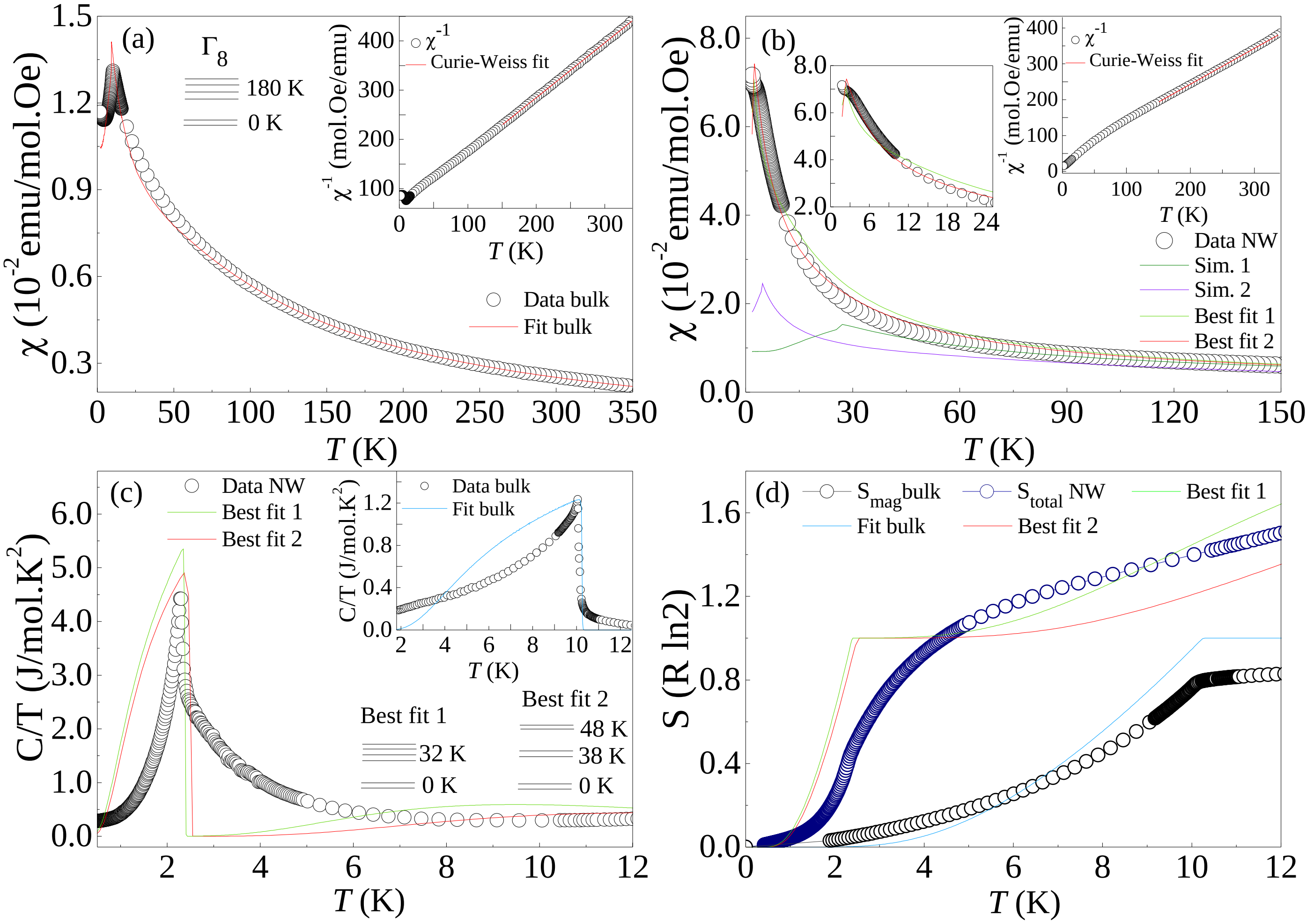

Fig. 3 (a, b) Temperature dependence of the magnetic susceptibility measured at $H = 0.1$ T for bulk and CeIn$_3$ nanowire, respectively. The solid lines are the fits/simulation to the data using the CEF mean field model discussed in the text. CEF energy levels splittings for the ground state of the Ce^{3+} obtained from fitting the experimental data is also shown. The inset of Fig 3(a,b) shows the Curie-Weiss fits in the inverse of susceptibility for bulk and nanowires, respectively. Fig. 3(c) show the specific heat data, and in Fig 3(d) the symbols show Total entropy for the NW and magnetic entropy (after subtracting the lattice contribution) for CeIn$_3$ bulk and the simulated entropy curves from the CEF model (lines).

of the CEF doublet ground state for the NW and/or the influence of short-range correlations. Furthermore, the evolution of entropy shows that roughly 1.5 $R\ln 2$ at 12 K, which indicates that the excited CEF Γ_8 quartet state is much lower in energy for the nanowires compared to bulk CeIn$_3$ [23,44,45]. The reduction of the energy of the CEF excited states has been claimed as one of the possible mechanisms for the reduction of T_N for the tetragonal AFM analogs Ce$_m$RhIn$_{3m+2}$ (m = 1,2) when compared to CeIn$_3$ [23]. This result should be interpreted with caution, since the nonmagnetic reference LaIn$_3$ for the NW system is not available to estimate phononic contributions in this system.

Figure 4 exhibits the specific heat divided by temperature C/T for CeIn$_3$ nanowires and bulk at zero magnetic field (Fig. 4(a)), and for CeIn$_3$ nanowires for different applied magnetic fields (Fig. 4(b)). It is worth noting that the magnetic transition in Fig. 4(b) broadens and changes its shape qualitatively. Further, the onset of the AFM order shifts towards lower temperatures upon increasing the magnetic field. This broadening is possibly associated with the presence of an inhomogeneous shift of T_N toward lower T due to disorder and/or diameter/internal field distribution in the arrangement of nanowires. In addition, a double peak feature can be observed for $H \geq 6$ T, which may also be a manifestation of disorder or, most likely, can be associated with a magnetic field-induced phase transition, similar to what was reported for the 115 compounds in [46].

3.3 Nuclear Magnetic Resonance

The full NMR spectrum measured at 2.3 K is shown in Fig. 5. Three main contributions were identified: the ^{63}Cu signal from the solenoid used in the measurement, the strong ^{27}Al signal from the Al$_2$O$_3$ template and the ^{115}In signal attributed to the CeIn$_3$ nanowires. The latter intensity was multiplied by a factor of 40 for clarity in the figure.

A significant difference is observed between the intensity of the ^{27}Al NMR signal and the ^{115}In NMR signal, which is mainly due to the amount of active nuclei in each specimen. Most of the NMR signal observed is from the alumina template because of its larger

View Article Online
DOI: 10.1039/D6NA00173D

Table 2 CEF parameters and energy levels separation, exchange interactions between nearest ($K_{Nearest}$) and next-nearest neighbors (K_{NNN}) and maximum temperature (T_{max}) obtained with the model for CeIn$_3$ nanowires and bulk.

	B_4^0	B_4^4	$K_{Nearest}$	K_{NNN}	T_{max} (K)	E. Split 1 (K)	E. Split 2 (K)
Bulk parameters	0.5	2.5	5.19	-0.63	10.0	180	—
Simulation 1	0.1	0.5	5.19	-0.63	30.6	36	—
Simulation 2	0.5	2.5	2.9	-0.18	4.6	180	—
Best fit 1	0.09	0.45	1.00	-0.16	2.3	32	—
Best fit 2	0.16	0.07	0.94	0.39	2.4	38	48

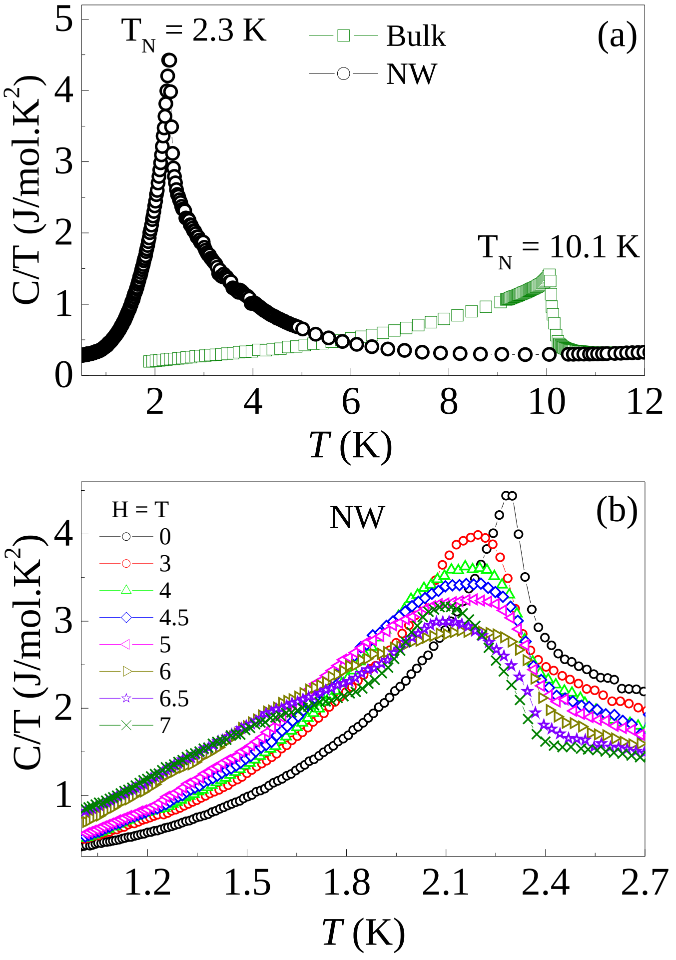

Fig. 4 (a) Specific heat of CeIn$_3$ nanowires and bulk plotted as $C/T \times T$, performed in 0 T and (b) Specific heat of CeIn$_3$ nanowires performed in different magnetic fields.

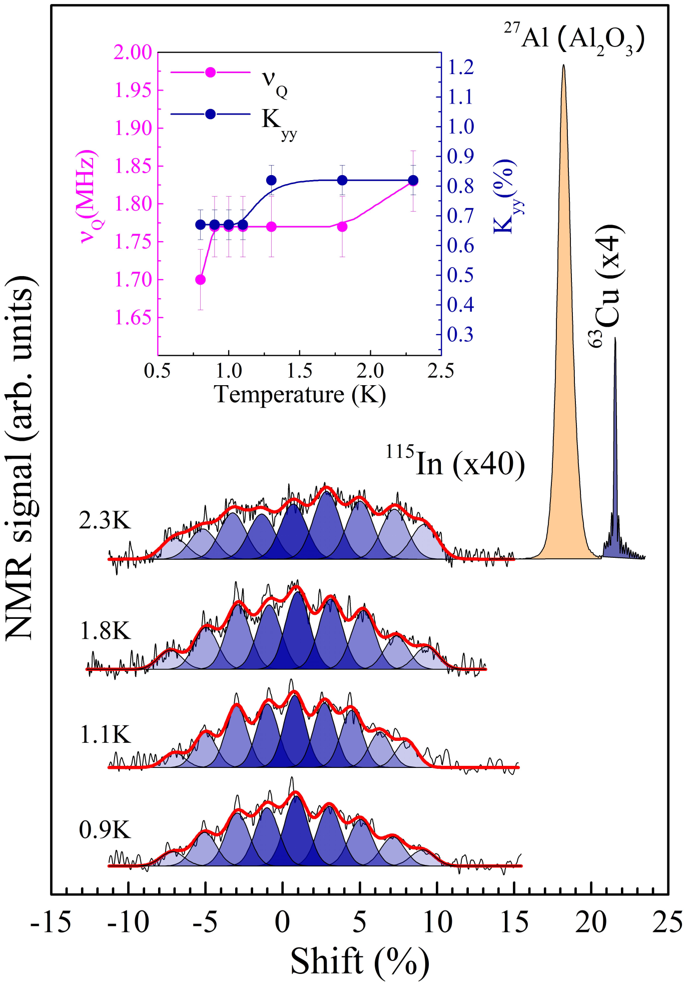

Fig. 5 FFT field swept NMR spectrum at 2.3 K showing the ^{63}Cu NMR signal from the solenoid (multiplied by 4), the ^{27}Al NMR signal from the alumina template and the ^{115}In NMR signal from the CeIn$_3$ nanowires (multiplied by 40). A few examples of low-T normalized ^{115}In NMR spectra as function of temperature are also presented. The inset highlights the Knight Shift $^{115}K_{yy}$ and the quadrupole resonance frequency ν_Q for $T \leq 2.3$ K.

mass, as expected. In the chosen frequency/field range, the ^{27}Al and ^{63}Cu NMR signals did not overlap and were used as reference for the ^{115}In NMR signal from the CeIn$_3$ nanowires.

Figure 5 also presents the ^{115}In NMR spectra at various temperatures. From the best fits with a convolution of 9 Gaussian lines, we extracted the values of the Knight shift, linewidth, and ν_Q as a function of temperature in the low-T regime around the AFM ordering temperature. The K and ν_Q temperature dependencies are shown in the inset of Fig. 5.

A noticeable change is observed in both parameters around $T \approx 1.8$ K at roughly 4.65 T, in general agreement with the antiferromagnetic order observed by specific heat measurements of our CeIn$_3$ nanowires under similar applied magnetic field.

Fig. 6 presents the ^{115}In NMR spectra obtained by sweeping up $H \parallel$ Al$_2$O$_3$ template at constant frequency ν = 43.1 MHz. The spectra present the typical features of a nuclear spin $I = 9/2$ with Zeeman and quadrupole couplings.

At low temperatures, the spectra show a broad central line with a full width at half maximum FWHM = 839 kHz (8.9 kOe) and four other broad satellite lines from each side split by the quadrupole interaction of the In nuclei with the local electric field gradient (EFG). The broad satellite lines are due to the strain in-

View Article Online
DOI: 10.1039/D6NA00173D

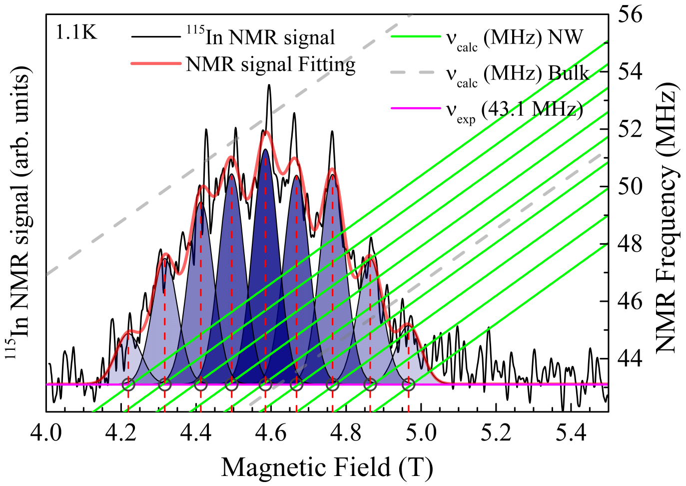

Fig. 6 ^{115}In NMR signal and fitting. The solid lines indicate the calculated frequencies as function of magnetic field for each resonance transition of the $I = 9/2$ nuclear spin system calculated after full diagonalization of the nuclear Hamiltonian. The gray (green) solid lines are calculated considering a $\nu_Q = 9.6$ MHz ($\nu_Q = 1.77(2)$ MHz) for the bulk (nanowires).

troduced by disorder, the different number of Ce neighbors to In sites, and the broadening of the central transition is due to the distribution of both hyperfine fields and EFG (as 2*nd* order contribution).

The quadrupole splitting is proportional to the EFG at the In site, V_{zz}, through the relation: $\nu_Q = eQV_{zz}/2\sqrt{1+\eta^2/3}$, where Q is the nuclear quadrupole moment of ^{115}In and η is the asymmetry parameter of the EFG ($\eta = 0$ for a tetragonal site symmetry). V_{zz} arises from the hybridization between the In-5d and the Ce-4f orbitals resulting in the quadrupole frequency, $\nu_Q = 1.77(2)$ MHz. Strikingly, this is roughly 5 times smaller than $\nu_Q = 9.6$ MHz observed in the bulk CeIn$_3$ single crystal[47]. This suppression in the quadrupole frequency suggests a major change in the EFG, and thus in the crystallographic parameters at low temperatures. This result is consistent with the changes in the CEF effects and the consequent changes in the Ce 4f CEF scheme of energy levels also suggested by the heat capacity data.

Because the quadrupole interaction is a substantial perturbation in the Hamiltonian, in order to fully characterize the ^{115}In spectra, we calculated the frequency as a function of applied magnetic field by exactly diagonalizing the **Zeeman + Quadrupole** Hamiltonian using the software *MagRes2000* 8.9. In Fig. 6 one can see the results of these simulations. We adjusted the Knight shift K_{yy} and the ν_Q, so that we had a match between the perceived peak positions of the ^{115}In NMR spectra and the center of the simulated curves projected at the constant measured frequency (magenta line at 43.1 MHz). The agreement between our results can be seen through the intersection points between the transversal green lines and the horizontal magenta one. These lines represent the energy of the transition between the In nuclei spin energy levels and the frequency at which the NMR experiment was carried out (43.1 MHz), respectively. Moreover, we also show in Fig.6 the In nuclei spin energy transitions for the CeIn$_3$ bulk sample through the dashed gray transversal lines, for comparison. This evidences the drastic suppression of ν_Q from 9.6 MHz (bulk) to 1.77(2) MHz (nanowires).

Furthermore, if one compares the suppression of T_N with the reduction of ν_Q, from bulk to nanowires, it is possible to verify that they roughly scale. In other words, $T_N^{bulk}/T_N^{nanowire} \approx 4.2$ is comparable to $\nu_q^{bulk}/\nu_q^{nanowire} \approx 5$, suggesting a possible correlation between these parameters. However, further ^{115}In NMR measurements on bulk CeIn$_3$ single crystals, under identical experimental conditions to those applied to the NWs, would be beneficial to establish a comprehensive microscopic comparison. Such a study remains a target for future investigations.

As suggested by the SAED data, our CeIn$_3$ nanowires are likely polycrystalline. Therefore, it should be considered that the peaks in the NMR data are dominated by crystallites whose Euler angle between the magnetic field and the local EFG's are at 90 degrees with each other, as assumed in the model calculation of Fig. 6. This then places a stringent upper bound to the resulting value of EFG. (i.e., the calculated EFG would be even lower if $\theta = 0$). Therefore, this scenario is consistent with the growth of the nanowires inside the alumina template, not quite aligned with respect to the uniaxial direction of the nanoporous.

The NMR results reported here clearly confirmed the presence of disordered AFM ordering and revealed a significant change in the charge distribution probed by the In nuclei in the CeIn$_3$ NW when compared to the bulk. This is clearly connected to changes in the Ce^{3+} CEF scheme going from the bulk to nanowires revealed by the evolution of the magnetic properties shown in Fig. 3.

To further analyze these results, it is important to notice that our model can satisfactorily capture the mean features of $\chi(T)$ and $C_p(T)$ data with their best fit using the parameters displayed in Table 2. To explore possible scenarios in order to understand the dramatic suppression of the AFM in the CeIn$_3$ NW, we have also performed several simulations considering various hypotheses.

In simulation 1, we kept the exchange parameters obtained for the best fits of the bulk CeIn$_3$ and employed a variation of the cubic CEF, B_4^0 and B_4^4 parameters, scaled by the variation of $\nu_q^{bulk}/\nu_q^{nanowire} \approx 5$, decreasing the overall CEF splitting as suggested by the $C_p(T)$ data in Fig. 3.

For simulation 2, we have scaled the exchange parameters using $T_N^{bulk}/T_N^{NW} \approx 4.2$ while keeping the cubic CEF, B_4^4 and B_4^0 parameters, constant as in the bulk. One can see that both simulations 1 and 2 are not capable of precisely reproducing the $\chi(T)$ for the CeIn$_3$ NW, suggesting that both the exchange interactions and CEF parameters are changing, presumably in a non-trivial way.

As such, we have performed fits to the data of Fig. 3 with and without keeping the cubic ratio $B_4^4/B_4^0 = 5$ as a constraint. By analyzing the best fits to the data, it becomes clear that both the CEF parameters (B_4^0 and B_4^4) and the exchange interaction parameters ($K_{Nearest}$ and K_{NNN}) (see Table 2) are significantly reduced in the CeIn$_3$ nanowires compared to the bulk. This reduction in the exchange interaction parameters is consistent with the decrease in θ_{CW} obtained from Curie–Weiss analysis. Furthermore, a more adequate fit is achieved by allowing free values for B_4^0 and

View Article Online
DOI: 10.1039/D6NA00173D

B_4^4, which suggests the presence of tetragonal distortion. Interestingly, it has been shown that the reduction of the energy of the CEF excited states in tetragonal symmetry can lead to a CEF induced magnetic frustration, which may play a role in the reduction of T_N for the tetragonal AFM analogs Ce$_m$RhIn$_{3m+2}$ (m = 1,2) when compared to CeIn$_3$ [23].

As such, the data provide substantial evidence that the Ce^{3+} local environment in the CeIn$_3$ nanowires is inhomogeneously distorted at low temperatures, indicating the presence of significant structural disorder in the nanowires. This behavior is consistent with the framework proposed by Barriga-Castro et al., in which the confined growth of nanowires inside the nanopores of the alumina template imposes geometric constraints that favor the formation of defects, such as stacking faults, and local lattice distortions[48]. For CeIn$_3$ nanowires, such confinement-induced disorder is expected to affect the relevant interactions. In particular, it can simultaneously reduce the exchange interaction, possibly decreasing the CEF splitting, and increasing the Kondo effect. It can be hypothesized that the aforementioned effects are collectively contributing to the frustration of the magnetic order in the CeIn$_3$ nanowires. Acquisition of low-T structural crystallographic measurements for CeIn$_3$ nanowires, while undeniably challenging, would undoubtedly yield invaluable insights, to confirm the proposed interpretation.

Conclusions

In this work, we have employed the Metallic-Flux Nanonucleation method to synthesize CeIn$_3$ nanowires (LD system) and studied their properties via macroscopic and microscopic measurements comparing the results with those obtained for CeIn$_3$ single crystals (bulk). The EDS analysis and the SAED pattern indexing confirmed that the nanowires show the cubic phase of CeIn$_3$ at room-T. Magnetic susceptibility, specific heat, and NMR data showed a drastic suppression of the antiferromagnetic transition from the bulk ($T_N^{3D} = 10.1$ K) to the nanowire system ($T_N^{LD} = 2.3$ K). Fits and simulations of these data, using mean field model with cubic and distorted CEF Hamiltonians and isotropic nearest neighbor exchange parameters, suggested a dramatic reduction of the exchange interaction and the CEF splitting, followed by a possible tetragonal distortion and increase of the Kondo effects for CeIn$_3$ nanowires at low temperature. Our findings suggest that the confinement of tunable complex strongly correlated materials in a nanoporous membrane can lead to dramatic changes in their properties even in a length scale range well above the quantum limit. This strongly motivates the use of the Metallic-Flux Nanonucleation method to study quantum materials prepared in nanowire form in a broader perspective.

Conflicts of interest

The authors declare that there is no conflict of interest.

Data availability

The data supporting this article have been included in the main text.

Acknowledgements

This work was financially supported by the Brazilian funding agencies Fundação de Amparo à Pesquisa do Estado de São Paulo (FAPESP, Grants No. 2022/16823-5, 2020/10580-8, and 2017/10581-1) and CNPq (Grants No. 308831/2025-0, 405408/2023-4, 314587/2021-7 and 311783/2021-0). A portion of this work was performed at the National High Magnetic Field Laboratory, which is supported by the National Science Foundation Cooperative Agreement No. DMR-2128556 and the State of Florida. We also acknowledge the electron microscopy support provided by LNNano – the Brazilian Nanotechnology National Laboratory (LNNano/CNPEM/MCTI) – and the Center for Integrated Nanotechnologies (CINT), an Office of Science User Facility operated for the U.S. Department of Energy, Office of Science. We further acknowledge support from the INCT project Advanced Quantum Materials, involving the Brazilian agencies CNPq (Proc. 408766/2024-7), FAPESP, and CAPES. The authors thank Winson Kuo for assistance with the Focused Ion Beam experiments, and Priscila F. S. Rosa and Joe Thompson for their significant contributions to this work.

Notes and references

1 P. Liu, J. R. Williams and J. J. Cha, *Nature Reviews Materials*, 2019, **4**, 479–496.
2 L. W. Martin and A. M. Rappe, *Nature Reviews Materials*, 2016, **2**, 1–14.
3 K. Pirota, K. Moura, A. da Cruz, R. Campanelli, P. Pagliuso and F. Béron, *Magnetic Nano- and Microwires*, Woodhead Publishing, Second Edition edn, 2020, pp. 61–84.
4 D. Tsivion, M. Schvartzman, R. Popovitz-Biro, P. Von Huth and E. Joselevich, *Science*, 2011, **333**, 1003–1007.
5 A. Fetter and J. Walecka, *Quantum Theory of Many-particle Systems*, Dover Publications, 2003.
6 F. W. Halperin, *Reviews of Modern Physics*, 1986, **58**, 533.
7 Y.-S. Fu, S.-H. Ji, X. Chen, X.-C. Ma, R. Wu, C.-C. Wang, W.-H. Duan, X.-H. Qiu, B. Sun, P. Zhang *et al.*, *Physical Review Letters*, 2007, **99**, 256601.
8 G. Wang, L.-S. Liu, Z. Zhu, Y. Zheng, B. Yang, D. Guan, S. Wang, Y. Li, C. Liu, W. Chen *et al.*, *Physical Review Letters*, 2025, **135**, 076201.
9 Q. Si and F. Steglich, *Science*, 2010, **329**, 1161–1166.
10 N. Berry, E. Bittar, C. Capan, P. Pagliuso and Z. Fisk, *Physical Review B-Condensed Matter and Materials Physics*, 2010, **81**, 174413.
11 T. Ebihara, N. Harrison, M. Jaime, S. Uji and J. Lashley, *Physical Review Letters*, 2004, **93**, 246401.
12 P. J. Moll, T. Helm, S.-S. Zhang, C. D. Batista, N. Harrison, R. D. McDonald, L. E. Winter, B. Ramshaw, M. K. Chan, F. F. Balakirev *et al.*, *Quantum Materials*, 2017, **2**, 46.
13 N. Mathur, F. Grosche, S. Julian, I. Walker, D. Freye, R. Haselwimmer and G. Lonzarich, *Nature*, 1998, **394**, 39–43.
14 F. Grosche, I. Walker, S. Julian, N. Mathur, D. Freye, M. Steiner and G. Lonzarich, *Journal of Physics: Condensed Matter*, 2001, **13**, 2845.

View Article Online
DOI: 10.1039/D6NA00173D

15 H. Shishido, T. Shibauchi, K. Yasu, T. Kato, H. Kontani, T. Terashima and Y. Matsuda, *Science*, 2010, **327**, 980–983.

16 S. Paschen and Q. Si, *Nature Reviews Physics*, 2021, **3**, 9–26.

17 Joe D. Thompson and Zachary Fisk, *Journal of the Physical Society of Japan*, 2012, **81**, 011002.

18 C. Petrovic, R. Movshovich, M. Jaime, P. G. Pagliuso, M. F. Hundley, J. L. Sarrao, Z. Fisk and J. D. Thompson, *Europhysics Letters*, 2001, **53**, 354.

19 C Petrovic, P G Pagliuso, M F Hundley, R Movshovich, J L Sarrao, J D Thompson, Z Fisk and P Monthoux, *Journal of Physics: Condensed Matter*, 2001, **13**, L337.

20 K. Buschow, H. De Wijn and A. Van Diepen, *The Journal of Chemical Physics*, 1969, **50**, 137–141.

21 M. Amara, R. Galera, P. Morin, T. Veres and P. Burlet, *Journal of magnetism and magnetic materials*, 1994, **130**, 127–132.

22 M. Amara, R. Galéra, P. Morin, J. Voiron and P. Burlet, *Journal of magnetism and magnetic materials*, 1995, **140**, 1157–1158.

23 P. G. Pagliuso, D. J. Garcia, E. Miranda, E. Granado, R. Lora Serrano, C. Giles, J. G. S. Duque, R. R. Urbano, C. Rettori, J. D. Thompson, M. F. Hundley and J. L. Sarrao, *Journal of Applied Physics*, 2006, **99**, 08P703.

24 W. Simeth, Z. Wang, E. Ghioldi, D. M. Fobes, A. Podlesnyak, N. Sung, E. D. Bauer, J. Lass, S. Flury, J. Vonka *et al.*, *Nature communications*, 2023, **14**, 8239.

25 P. Rosa, L. de Oliveira, C. de Jesus, K. Moura, C. Adriano, W. Iwamoto, T. Garitezi, E. Granado, M. Saleta, K. Pirota and P. Pagliuso, *Solid State Communications*, 2014, **191**, 14–18.

26 M. H. Carvalho, G. S. Freitas, J. C. Souza, R. B. Campanelli, H. B. Pizzi, S. G. Mercena, M. Puydinger dos Santos, F. Béron, P. F. S. Rosa, K. Pirota and P. G. Pagliuso, *Journal of Physics: Conference Series*, 2022, **2164**, 012041.

27 S. Tang, J. Tang, Y. Wu, Y.-H. Chen, J. Uzuhashi, T. Ohkubo and L.-C. Qin, *Nanoscale*, 2021, **13**, 17156–17161.

28 H. Zhang, Y. Jimbo, A. Niwata, A. Ikeda, A. Yasuhara, C. Ovidiu, K. Kimoto, T. Kasaya, H. T. Miyazaki, N. Tsujii *et al.*, *Nature nanotechnology*, 2022, **17**, 21–26.

29 M. Gou, S. Tang, K. Huang, H. Guan, R. Zhan, C. Liang, C. Chen, Y. Shen and S. Deng, *Communications Materials*, 2025, **6**, 133.

30 K. Moura, L. De Oliveira, P. F. S. Rosa, C. Jesus, M. Saleta, E. Granado, F. Béron, P. Pagliuso and K. Pirota, *Scientific reports*, 2016, **6**, 28364.

31 K. O. Moura, K. R. Pirota, F. Béron, C. B. Jesus, P. F. S. Rosa, D. Tobia, P. Pagliuso and O. d. Lima, *Scientific reports*, 2017, **7**, 15306.

32 E. Alexsandro dos Santos, M. V. P. Dos Santos, R. B. Campanelli, P. G. Pagliuso, J. Bettini, K. R. Pirota and F. Béron, *Nanoscale advances*, 2021, **3**, 3251–3259.

33 A. S. Cruz, R. B. Campanelli, M. V. P. Dos Santos, F. Fabris, J. Bettini, P. G. Pagliuso and K. R. Pirota, *Nanotechnology*, 2022, **33**, 475704.

34 R. B. Campanelli, M. V. P. dos Santos, A. S. E. da Cruz, K. R. Pirota and F. Béron, *IEEE Transactions on Nanotechnology*, 2021, **20**, 739–743.

35 K. Pirota, F. Beron, L. Oliveira, K. Moura, M. Knobel, P. G. Pagliuso, T. Garitezi, C. de Jesus, C. Rettori, C. Adriano, P. Rosa, R. R. Urbano, W. Iwamoto, L. Arzuza and P. Carvalho, *BR 10 2014 019794 0*, 2014, 2014.

36 Z. Fisk and J. P. Remeika., *Elsevier Science Publishers*, 1989, **12**, chapter 81 edition.

37 W. Lee, R. Ji, U. Gösele and K. Nielsch, *Nature materials*, 2006, **5**, 741–747.

38 G. S. Freitas, M. M. Piva, R. Grossi, C. B. R. Jesus, J. C. Souza, D. S. Christovam, N. F. Oliveira Jr, J. B. Leão, C. Adriano, J. W. Lynn and P. G. Pagliuso, *Physical Review B*, 2020, **102**, 155129.

39 D. S. Christovam, G. S. Freitas, M. M. Piva, J. C. Souza, M. O. Malcolms, O. L. Canton, J. B. Leão, W. Ratcliff, J. W. Lynn, C. Adriano and P. G. Pagliuso, *Physical Review B*, 2020, **102**, 195137.

40 K W H Stevens, *Proceedings of the Physical Society. Section A*, 1952, **65**, 209.

41 E. G. Moshopoulou, R. M. Ibberson, Sarrao, J. L., J. D. Thompson and Z. Fisk, *Acta Crystallographica Section B*, 2006, **62**, 173–189.

42 A. W. Thompson, Z. D. Harris and J. T. Burns, *Micron*, 2019, **118**, 43–49.

43 S. Blundell, *Magnetism in Condensed Matter*, OUP Oxford, Oxford, 2nd edn, 2001.

44 J. Lawrence and S. Shapiro, *Physical Review B*, 1980, **22**, 4379.

45 W. Knafo, S. Raymond, B. Fåk, G. Lapertot, P. Canfield and J. Flouquet, *Journal of Physics: Condensed Matter*, 2003, **15**, 3741.

46 J. Duque, R. L. Serrano, D. Garcia, L. Bufaical, L. Ferreira, P. Pagliuso and E. Miranda, *Journal of magnetism and magnetic materials*, 2011, **323**, 954–956.

47 Y. Kohori, Y. Inoue, T. Kohara, G. Tomka and P. Riedi, *Physica B: Condensed Matter*, 1999, **259**, 103–104.

48 E. D. Barriga-Castro, J. García, R. Mendoza-Reséndez, V. M. Prida and C. Luna, *RSC advances*, 2017, **7**, 13817–13826.

View Article Online
DOI: 10.1039/D6NA00173D

Data Availability Statement

The data supporting this article have been included in the main text.